

Communication

Gain-Switched Er-Doped Fluoride Fiber Laser at $\sim 3.75 \mu\text{m}$

Lu Zhang ^{1,2}, Shijie Fu ^{1,2,*}, Quan Sheng ^{1,2}, Xuewen Luo ^{1,2}, Junxiang Zhang ^{1,2}, Wei Shi ^{1,2,*}, Qiang Fang ³ and Jianquan Yao ^{1,2}

- ¹ Institute of Laser and Optoelectronics, School of Precision Instrument and Optoelectronics Engineering, Tianjin University, Tianjin 300072, China; zlu@tju.edu.cn (L.Z.); shengquan@tju.edu.cn (Q.S.); lxw_520@tju.edu.cn (X.L.); junxiang@tju.edu.cn (J.Z.); jqyao@tju.edu.cn (J.Y.)
- ² Key Laboratory of Opto-Electronic Information Technology, Ministry of Education, Tianjin University, Tianjin 300072, China
- ³ HFB Photonics Co., Ltd., Weihai 264209, China; fangq@hfbphotonics.com
- * Correspondence: shijie_fu@tju.edu.cn (S.F.); shiwei@tju.edu.cn (W.S.)

Abstract: We demonstrate a pulsed Er-doped ZBLAN fiber laser operating at $3.75 \mu\text{m}$ based on the gain-switching scheme. A diffraction grating is introduced as a wavelength selection component to enable stable lasing in this long-wavelength region that deviates from the emission peak of ${}^4\text{F}_{9/2} \rightarrow {}^4\text{I}_{9/2}$ transition in Er^{3+} . Different from the conventional gain-switching behavior where the pulse repetition frequency of the output laser is same as the that of the pump, the gain-switched laser demonstrated here shows a variable pulse repetition frequency, which accounts for $1/n$ ($n = 4, 3, 2$) of the pump pulse repetition frequency, in response to the 1950 nm pump power. The output pulse characteristics, including average output power, repetition frequency, pulse duration, and peak power, are investigated in detail. Over 200 mW average output power at $3.75 \mu\text{m}$ was obtained at 12 W of 1950 nm pump power. This work demonstrates that the Er-doped ZBLAN fiber laser, in combination with gain-switched scheme, is a feasible and promising approach to generate powerful pulsed emission $> 3.7 \mu\text{m}$.

Keywords: mid-infrared fiber laser; gain-switching; Er; fluoride fiber



Citation: Zhang, L.; Fu, S.; Sheng, Q.; Luo, X.; Zhang, J.; Shi, W.; Fang, Q.; Yao, J. Gain-Switched Er-Doped Fluoride Fiber Laser at $\sim 3.75 \mu\text{m}$. *Photonics* **2024**, *11*, 449. <https://doi.org/10.3390/photonics11050449>

Received: 9 April 2024
Revised: 6 May 2024
Accepted: 10 May 2024
Published: 11 May 2024



Copyright: © 2024 by the authors. Licensee MDPI, Basel, Switzerland. This article is an open access article distributed under the terms and conditions of the Creative Commons Attribution (CC BY) license (<https://creativecommons.org/licenses/by/4.0/>).

1. Introduction

Recent attention has been devoted to developing mid-infrared fiber lasers, driven by a number of applications in medicine, remote sensing, material processing, laser filamentation, and high-energy-density physics [1–6]. The wavelength region of $3.7\text{--}4 \mu\text{m}$, which overlaps with both the atmosphere transparency window and the specific ‘fingerprint’ absorption region of harmful gas, such as H_2S , is of particular interest in such applications as free-space communication and dangerous gas detections [7,8]. Although $\sim 200 \text{ mW}$ at $3.92 \mu\text{m}$ was demonstrated early in 2018 with a holmium-doped fluorindate fiber laser, the lasing is potentially self-terminated given the long-lived lower laser level [9]. ${}^4\text{F}_{9/2} \rightarrow {}^4\text{I}_{9/2}$ transition in Er-doped ZBLAN fiber benefiting a wide fluorescence spectrum extending above $3.8 \mu\text{m}$ and the absence of self-termination effect [10] make it another promising routine for powerful long-wavelength emission. The development of double-cladding Er-doped fluoride fibers and fiber Bragg grating (FBG) inscription technology has contributed to many remarkable progress in laser demonstrations based on this transition, namely 15 W at $3.55 \mu\text{m}$ [11] and 1.2 W at $3.79 \mu\text{m}$ [12]. Wide wavelength tuning over a span of 450 nm ($3330\text{--}3780 \text{ nm}$) in multi-longitudinal mode regime [13] and 344.7 nm ($3373.8\text{--}3718.5 \text{ nm}$) in single-longitudinal mode regime [14] has also been demonstrated in diffraction grating-based configurations.

Although the power scaling and wavelength extension potential of the Er-doped ZBLAN fiber lasers have been demonstrated in continuous-wave (CW) regime, pulsed laser generation beyond $3.7 \mu\text{m}$ with high output power is still an ongoing challenge.

Such pulsed fiber lasers with high energy and high peak power are strongly demanded in some specific applications, like laser surgery, supercontinuum generation, and nonlinear optics [15–17]. However, there are two main factors that hinder the development of pulsed Er-doped fiber laser at $>3.7 \mu\text{m}$. The first thing is the decreasing emission cross-section of ${}^4\text{F}_{9/2} \rightarrow {}^4\text{I}_{9/2}$ transition, which exhibits $\sim 40\%$ reduction at 3700 nm and $\sim 80\%$ reduction at 3800 nm, respectively, compared with its peak value at $\sim 3.47 \mu\text{m}$. This results in a very limited long-wavelength laser gain and induces strong gain competition. On the other hand, the typical actively Q-switching method for pulsed laser generation, like electro-optic or acousto-optic Q-switching approaches, is less studied in the mid-infrared region due to the lack of temporal modulation devices. Passive Q-switching is another routine and several materials have been developed as a saturable absorber to generate mid-infrared pulsed laser. In 2019, H. Luo et al. reported a 3407.2–3701.1 nm tunable pulsed Er-doped ZBLAN fiber laser, in which the intracavity field was passively Q-switched by a Fe:ZnSe crystal [18]. This is, to our knowledge, the only one-pulsed rare-earth-doped fiber laser demonstration with operating wavelength extending beyond 3700 nm. However, the employment of an intracavity modulation element would increase both the cavity loss and complexity in optical alignment, which compromises the laser performance and constrains laser wavelength extension to the low-gain region. The potential risk of device damage also prevents power scaling from high pump power. Owing to these issues, the average output power at the emission peak wavelength of 3478 nm was limited to 584 mW, and quickly decreased to 70 mW with the emission wavelength tuned to 3701 nm. It is worth mentioning that when the $\text{Fe}^{2+}:\text{ZnSe}$ crystal and the confocal scheme were removed from the cavity, the CW lasing wavelength could be further extended to 3730.6 nm under the same pump condition. The comparison highlights the importance of low cavity loss for extending laser wavelength to the low-gain region.

A promising candidate to meet this requirement is the gain-switching method, in which the laser cavity is directly pumped by a pulsed laser. This scheme is simple, compact, and more favorable for long-wavelength lasing, since no additional intracavity modulators are needed. However, a gain-switched laser also has its shortcomings, for example, the essential pulsed pump source is usually expensive and not easy to realize. Additionally, compared with active Q-switching, the pulse characteristics, like pulse duration and repetition frequency, of the gain-switched fiber laser usually cannot be flexibly adjusted. Nevertheless, mid-infrared pulsed fiber lasers have made significant progress in output power via the gain-switching method, with 11.2 W at $2.826 \mu\text{m}$ (${}^4\text{I}_{11/2} \rightarrow {}^4\text{I}_{13/2}$) [19] and 1.04 W at $3.46 \mu\text{m}$ (${}^4\text{F}_{9/2} \rightarrow {}^4\text{I}_{9/2}$) [20]. Note that both of these two demonstrations are carried out within the strong-emission region of Er-doped ZBLAN fiber. At longer wavelength near $3.7 \mu\text{m}$, only one gain-switched fiber laser demonstration was reported by J. Yang et al., in which the laser cavity was arranged with a diffraction grating-based configuration and yielded a tunable wavelength up to 3690.2 nm [21]. It should be noted that the laser employed two 1981 nm pumps, namely one CW pump for reaching the threshold first, and the other pulsed pump for gain-switching. This design increased the system complexity and the misalignment-induced cavity loss, which, combined with the diminishing emission cross-section, resulted in a similar laser performance as the Q-switched one mentioned above [18], i.e., output power decreased significantly at longer wavelength, with average output power $<50 \text{ mW}$ at 3690.2 nm.

Here, we demonstrated a further wavelength extension of such a gain-switched Er-doped ZBLAN fiber laser. The laser was pumped by a homemade high-power pulsed 1950 nm fiber laser and yielded 238 mW average output power at a lasing wavelength of $3.75 \mu\text{m}$. Three switchable stable gain-switched temporal states with output PRF quartering, trisecting, and halving with respect to the pump source are observed in the experiment. At the maximum pump power, the pulse duration, energy, and peak power are 1.2 μs , 6.7 μJ , and 5.6 W, respectively. Our work demonstrated the potential of Er: ZBLAN fiber laser system to achieve efficient long-wavelength pulsed laser emission, paving the way for

mid-infrared fiber lasers for a broad range of practical applications from communications and sensing to scientific research.

2. Experimental Setup

Figure 1a depicts the experimental setup of the gain-switched Er-doped ZBLAN fiber laser. The laser employed a 976 nm + 1950 nm dual-wavelength pumping scheme and the involved energy transitions are shown in Figure 1b. The Er-doped ZBLAN fiber was first pumped at 976 nm via the ground state absorption (GSA) to create an initial ion accumulation in the long-lived $^4I_{11/2}$ level (virtual ground state, VGS), from which the Er ions were further promoted to the $^4F_{9/2}$ level via the virtual ground state absorption (VGSA) at 1950 nm and the gain-switched pulse emission was generated via $^4F_{9/2} \rightarrow ^4I_{9/2}$ transition. Note that the 1950 nm pump can also be consumed by a deleterious ESA ($^4F_{9/2} \rightarrow ^4F_{7/2}$, centered at 1913 nm), which would impair the population inversion and cause strong laser quenching behavior [22]. Mitigating this issue requires a high pump power of 976 nm to provide enough Er ions to populate the $^4I_{11/2}$ level, enabling the absorption of the 1950 nm pump to be dominated by the VGSA. In our design, the 976 nm pump was a 20 W multimode laser diode, while the 1950 nm pump was a homemade pulsed Tm-doped fiber laser, consisting of a pulsed fiber laser seed [23] and three stage amplifiers, which provided a maximum output power of 15 W. The PRF and pulse duration were 72 kHz and 1.4 μ s, respectively. The 976 nm and 1950 nm pump lasers were first collimated by two aspheric lenses (L1: $f = 8$ mm and L4: $f = 15$ mm) and then individually focused and launched into the gain fiber from both ends through two CaF₂ lenses (L2 and L3: $f = 12.7$ mm). The 976 nm pump was launched into the inner cladding, while the 1950 nm pump propagated in the fiber core for a large mode field overlap and sufficient absorption. Such a bidirectional pumping scheme helped to spread the thermal load and allowed us to use higher pump power for output power scaling. The gain medium was a segment of 5.5 m 1 mol.% Er-doped ZBLAN fiber ($16.5/260 \times 240$ μ m, NA = 0.125, Le Verre Fluoré, Bruz, France) with both end facets perpendicularly cleaved, in which one end near the 1950 nm pump was butted to a dielectric mirror (DM2, coated for highly transmissive (HT) at 1950 nm and 976 nm and R = 67% @ 3.3–4 μ m) for cavity feedback and laser output. The distance between the DM2 coating surface and the fiber facet was 15 μ m. The intracavity laser from the other end was collimated using L3 and then resonated by a diffraction grating (GR1325-30035, Thorlabs, Newton, NJ, USA) arranged in Littrow configuration, where the first-order diffraction was used as narrow-band feedback for wavelength selection. The DM4 (coated for HT at 976 nm and HR at 1950 nm) was used to remove the residual 1950 nm pump and protect the 976 nm LD. The output laser was collimated and reflected from the pump road by DM1 (coated for HT at 1950 nm and 976 nm and HR @ 3.3–4 μ m), and then purified using a long-pass filter (LPE, >3 μ m) to remove the backward pump and the possible 2.8 μ m parasitic lasing before measurement.

A wavelength-insensitive thermal power meter (12A, Ophir, Jerusalem, Israel) was used to measure the output power. The temporal behavior of the gain-switched laser was measured simultaneously from the 0th-order diffraction of the grating by a four-channel oscilloscope (DPO2024B, Tektronix, Beaverton, OR, USA) incorporating a HgCdTe (MCT) detector with 1 MHz bandwidth (PDAVJ5, Thorlabs, Newton, NJ, USA).

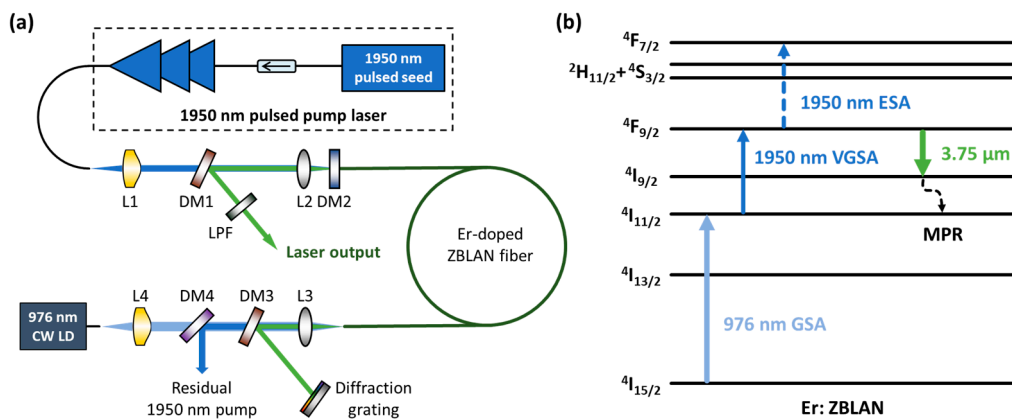


Figure 1. (a) Experimental setup of our gain-switched Er-doped fiber laser. DM1–DM4: dichroic mirrors; L1 and L4: aspheric lens; L2 and L3: CaF₂ biconvex lens, LPF: long-pass filter. (b) Energy level diagram of Er-doped ZBLAN fiber only involving the processes of pump absorption, laser transition, and multiphonon relaxation (MPR). GSA: ground state absorption; VGSA: virtual ground state absorption; ESA: excited state absorption.

3. Results and Discussion

We first measured the coupling efficiencies of the 1950 nm pump (to fiber core) and 976 nm pump (to fiber inner cladding). In the case without the 976 nm pump, the Er-doped ZBLAN fiber had no absorption on the 1950 nm pump and ~89% of the 1950 nm pump can transmit through the Er-doped ZBLAN fiber. The reduced 10% power was due to the Fresnel reflection (~4%) at two fiber facets and the ZBLAN fiber background loss (13.5 dB/km @ 1950 nm). Taking these losses into account, the effective 1950 nm pump coupling efficiency was estimated at 98%. Increasing the 976 nm pump power effectively populated the ⁴I_{11/2} level, leading to a strong absorption of 1950 nm pump power. Eventually, ~12% of the 1950 nm pump power could still be detected at the output end. The residual pump power is attributed to the fact that a small fraction of pump light was coupled into the inner cladding, which experienced a much weaker VGSA. Based on this value, it is estimated that 88% of the 1950 nm pump laser coupled into the fiber propagates inside the fiber core. The 976 nm pump coupling efficiency is difficult to measure using Er-doped ZBLAN fiber due to the strong GSA (ground state absorption) of Er³⁺ at 976 nm. Here, we replaced the Er-doped ZBLAN fiber with its passive matched ZBLAN fiber (14/250 μm) that has no absorption at 976 nm to measure the coupling efficiency. With the same management discussed above, the 976 nm pump coupling efficiency (to fiber cladding) is around 97.6%.

The output power of the gain-switched fiber laser was investigated with the grating wavelength tuned to ~3.75 μm. Considering the decreased emission cross-section, long-wavelength lasing requires higher population inversion, but populates fewer ions in VGS ⁴I_{11/2}. This results in a more serious quenching behavior, and thus demands higher 976 nm pump power compared with the ~3.47 μm laser case. Here, the 976 nm pump power was fixed at 14 W, under which the ~3.75 μm average output power as a function of incident 1950 nm pump power is shown in Figure 2a. Note that all the pump power mentioned in this paper refers to the 1950 nm pump measured behind L2. Compared with our previous 3.47 μm laser demonstrations with similar cavity arrangement [13], the long-wavelength laser here exhibited a significant threshold increment to a level of 5.5 W and a low slope efficiency of only 3.7%, which was attributed to the decreased emission cross-section and the unoptimized VGSA pump wavelength. Higher laser efficiency can be anticipated through the use of longer pump wavelength (e.g., 1990 nm) with good balance between VGSA and ESA [22], as well as the use of low-loss intracavity elements. The laser yielded 238 mW average output power when 12 W 1950 nm pump power was launched, and the corresponding laser spectrum was measured using an optical spectrum analyzer (OSA,

Bristol, 771B-MIR) with a resolution of 2 GHz (0.09375 nm @ 3.75 μm). As shown in Figure 2b, the central wavelength and the linewidth at FWHM were 3748.49 nm and 0.11 nm, respectively. Note that the optical signal-to-noise ratio (OSNR) here is below 20 dB and much lower than that measured in CW fiber laser [13]. The low OSNR can be explained in part by the strong gain competition at emission peak, and the compromised response of the OSA when measuring the pulsed laser with PRF < 50 kHz.

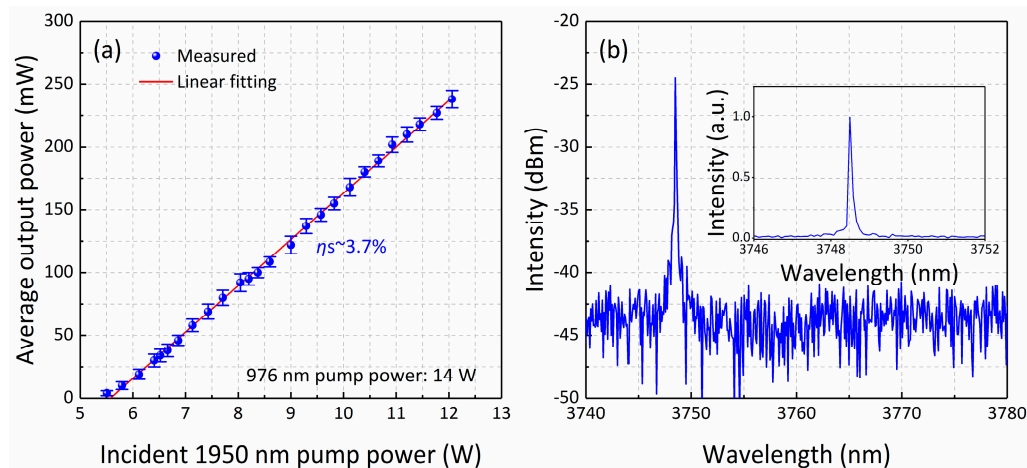


Figure 2. (a) Measured 3.75 μm average output power as a function of incident 1950 nm pump power; the error bars indicate the standard deviation of the output power with the mean average power. (b) Laser spectrum at maximum pump power. Inset: zoomed spectrum in linear scale.

The oscilloscope traces at different 1950 nm pump powers are shown in Figure 3, where the 1950 nm pulse trace was also presented for comparison. When the 1950 nm pump power was increased to 5.52 W, the pulsing behavior began with a periodic low-amplitude fluctuation, as shown in Figure 3a. It has a PRF of 72 kHz, i.e., the same as that of the pump, so it is confirmed that such a fluctuation indeed originated from the gain-switching, instead of self-pulsing or other processes. However, we still did not observe any optical spectral peak from the OSA, indicating that the fluctuation actually belongs to the weak amplified spontaneous emission (ASE). In other words, the population inversion (between $^4\text{F}_{9/2}$ and $^4\text{I}_{9/2}$) accumulated during each pump pulse would be quickly depleted by the spontaneous emission and other ETU processes, generating pulse-like fluctuation with same PRF as the pump. With higher pump power to enhance the population inversion, sporadic pulses with narrower duration and higher amplitude emerged, however, as a chaotic state where the pulse intensities and time intervals between adjacent pulses are in sustained variations, as shown in Figure 3b. As the pump power was further increased to 6.41 W, a stable 3.75 μm gain-switched pulse with higher SNR was obtained, as shown in Figure 3c. It is found that the PRF of the gain-switched pulse is only 18 kHz, i.e., a quarter of the pump's PRF, indicating that every four pump pulses generated one gain-switched pulse. Here, we named this state the "4-1" state. Such behavior was due to the fact that the 1950 nm pump has low pulse energy, and therefore, multiple pump cycles are required to gather enough population inversion to reach the pulsed laser threshold. However, the "n-1" state ($n \geq 5$) was not observed in our experiment, revealing that at lower pump power, the ions excited by the pump were mainly consumed through ASE, multi-phonon relaxation, and ETU, preventing the population of the $^4\text{F}_{9/2}$ level from ever reaching the lasing threshold.

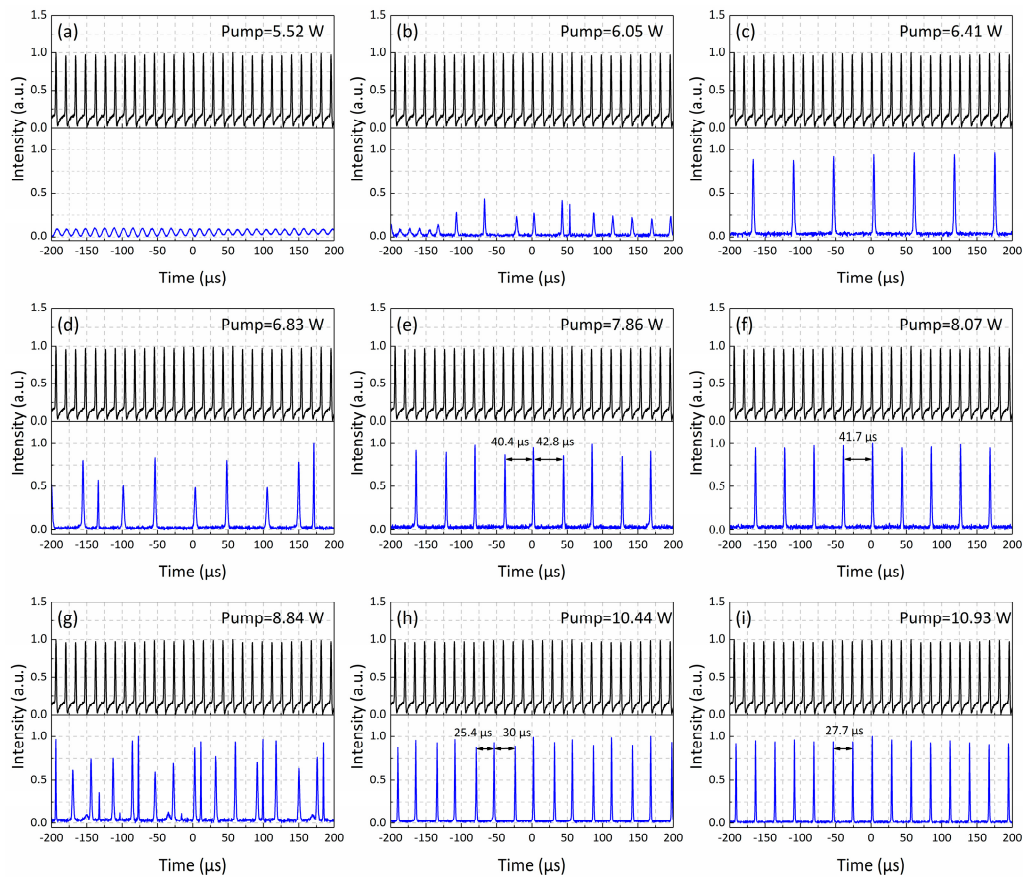


Figure 3. Sequential oscilloscope traces of the 3.75 μm gain-switched fiber laser (shown in blue) at 1950 nm pump powers (shown in black) of (a) 5.52 W, (b) 6.05 W, (c) 6.41 W, (d) 6.83 W, (e) 7.86 W, (f) 8.07 W, (g) 8.84 W, (h) 10.44 W, and (i) 10.93 W.

The “4-1” state can only be maintained at the 1950 nm pump below 6.66 W, and further increase in the pump power to 6.83 W resulted in a chaotic gain-switching process with serious timing jitter and amplitude fluctuation, as shown in Figure 3d, since the periodical balance between population accumulation and consumption of $^4F_{9/2}$ level was broken. As the 1950 nm pump power was increased to ~ 7.86 W, stable gain-switching was realized again but with a PRF of 24 kHz, indicating that just three pump pulses could provide enough population inversion, owing to the boosted pump pulse energy. Accordingly, this state was named the “3-1” state. It was found that the pulse intensity exhibited a periodical rise and fall, and the time intervals between two adjacent pulses were also different, periodically switching between 40.4 μs and 42.8 μs . These periodical behaviors were finally unified as the pump power was increased to 8.07 W, as shown in Figure 3f. This state could be maintained until the pump power increased to 8.6 W and the chaotic pulse trace appeared again at higher pump power, as shown in Figure 3g. When the pump power was further increased to 10.44 W, stable gain-switched pulses recovered with a PRF of 36 kHz, i.e., the “2-1” state, as shown in Figure 3h. Similar to the beginning of the “3-1” case, there were also two different time intervals (25.4 μs and 30 μs) between each of the two adjacent pulses, along with a periodic change in pulse intensity. Further increasing the pump power to 10.93 W led to a uniform pulse trace with same time interval (27.7 μs) and pulse intensity, as shown in Figure 3i. This “2-1” state could be maintained up to the maximum 1950 nm pump power. In this case, one gain-switched laser pulse was yielded after two pump pulses. Unfortunately, standard “1-1” gain switching, i.e., one pump pulse generating one gain-switched pulse, was not achieved in the experiment, owing to the high emission threshold at 3.75 μm , which cannot be reached with just a single pump pulse under the current experimental condition.

Figure 4a shows pulse duration, energy, and peak power of the 3.75 μm gain-switched laser as a function of incident 1950 nm pump power, where only the stable states are presented. Due to the increased population inversion between ${}^4\text{F}_{9/2}$ and ${}^4\text{I}_{9/2}$, the pulse energy and peak power increased monotonically, while the pulse duration decreased with the 1950 nm pump power. At the maximum pump power of 12 W, the pulse energy and duration were 6.7 μJ and 1.2 μs , respectively, corresponding to a peak power of 5.6 W. In this case, the zoomed single pulse shape of the 1950 nm pump laser and 3.75 μm gain-switched laser is shown in Figure 4b,c. Both the pulse energy and the duration did not exhibit saturation, indicating that gain-switching operation with higher pulse energy and shorter pulse duration can be anticipated by further increasing the pump power.

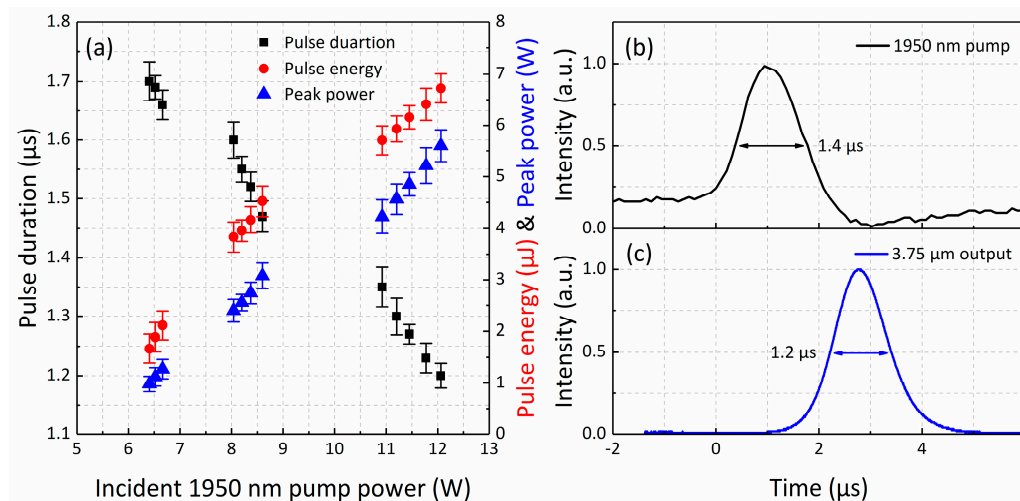


Figure 4. (a) Pulse duration, energy, and peak power of 3.75 μm gain-switched laser as a function of the incident 1950 nm pump power; the error bars indicate the standard deviation of the pulse duration, pulse energy, and peak power with the corresponding mean values. Zoomed single pulse shape of (b) 1950 nm pump laser and (c) 3.75 μm gain-switched laser at the maximum pump power.

4. Conclusions

In conclusion, we have demonstrated the first gain-switched Er-doped ZBLAN fiber laser operating above 3.7 μm . With the increase in the 1950 nm pulsed pump power, three switchable gain-switching states with output PRF quartering, trisecting, and halving with respect to the pump source were observed and characterized in detail. At the maximum 1950 nm pump power of 12 W, the laser yielded a maximum average output power of 238 mW at 3.75 μm , and the corresponding pulse energy, pulse duration, and peak power were 6.7 μJ , 1.2 μs , and 5.6 W, respectively. Its high energy and peak power make our demonstrated laser a good pump candidate for chalcogenide glass Raman fiber laser to generate >4 μm long-wavelength emission. Further performance improvement of the mid-infrared pulsed laser can be anticipated with optimized pump parameters.

Author Contributions: Conceptualization, L.Z. and S.F.; methodology, L.Z. and Q.S.; investigation, L.Z. and X.L.; resources, J.Z. and Q.F.; writing—original draft preparation, L.Z.; writing—review and editing, S.F.; supervision, S.F.; project administration, W.S.; funding acquisition, J.Y. All authors have read and agreed to the published version of the manuscript.

Funding: This research was funded by the National Natural Science Foundation of China (62375201, 62105240, 62075159, and 62275190), the Shandong Province Key R&D Program (2020CXGC010104, 2021CXGC010202), and the Seed Foundation of Tianjin University (2023XPD-0020).

Institutional Review Board Statement: Not applicable.

Informed Consent Statement: Not applicable.

Data Availability Statement: The data presented in this study are available from the corresponding authors upon reasonable request.

Conflicts of Interest: Author Qiang Fang was employed by the company HFB Photonics Co., Ltd. The remaining authors declare that the research was conducted in the absence of any commercial or financial relationships that could be construed as a potential conflict of interest.

References

1. Lee, B.G.; Belkin, M.A.; Audet, R.; MacArthur, J.; Diehl, L.; Pflügl, C.; Capasso, F.; Oakley, D.C.; Chapman, D.; Napoleone, A.; et al. Widely tunable single-mode quantum cascade laser source for mid-infrared spectroscopy. *Appl. Phys. Lett.* **2007**, *91*, 231101. [[CrossRef](#)]
2. Scherer, J.J.; Paul, J.B.; Jost, H.J.; Fischer, M.L. Mid-IR difference frequency laser-based sensors for ambient CH₄, CO, and N₂O monitoring. *Appl. Phys. B* **2013**, *110*, 271–277. [[CrossRef](#)]
3. Werle, P.; Slemr, F.; Maurer, K.; Kormann, R.; Mucke, R.; Janker, B. Near- and midinfrared laser-optical sensors for gas analysis. *Opt. Lasers Eng.* **2002**, *37*, 101–114. [[CrossRef](#)]
4. Bernier, M.; Fortin, V.; Caron, N.; El-Amraoui, M.; Messaddeq, Y.; Vallée, R. Mid-infrared chalcogenide glass Raman fiber laser. *Opt. Lett.* **2013**, *38*, 127–129. [[CrossRef](#)] [[PubMed](#)]
5. Fedorov, V.Y.; Tzortzakos, S. Powerful terahertz waves from long-wavelength infrared laser filaments. *Light Sci. Appl.* **2020**, *9*, 186. [[CrossRef](#)] [[PubMed](#)]
6. Migal, E.; Mareev, E.; Smetanina, E.; Duchateau, G.; Potemkin, F. Role of wavelength in photocarrier absorption and plasma formation threshold under excitation of dielectrics by high-intensity laser field tunable from visible to mid-IR. *Sci. Rep.* **2020**, *10*, 14007. [[CrossRef](#)] [[PubMed](#)]
7. Wang, B.; Cheng, B.; Zhao, W.; Li, Z.; Ji, X. Research on Directional Jamming to IR Imaging Seeker by 3.8 μm Laser. *Infrared* **2016**, *37*, 30–35.
8. Krier, A.; Sherstnev, V.V.; Gao, H. A novel LED module for the detection of H₂S at 3.8 μm . *J. Phys. D Appl. Phys.* **2000**, *33*, 1656–1661. [[CrossRef](#)]
9. Maes, F.; Fortin, V.; Poulain, S.; Poulain, M.; Carree, J.-Y.; Bernier, M.; Vallée, R. Room-temperature fiber laser at 3.92 μm . *Optica* **2018**, *5*, 761–764. [[CrossRef](#)]
10. Henderson-Sapir, O.; Munch, J.; Ottaway, D.J. Mid-infrared fiber lasers at and beyond 3.5 μm using dual-wavelength pumping. *Opt. Lett.* **2014**, *39*, 493–496. [[CrossRef](#)] [[PubMed](#)]
11. Lemieux-Tanguay, M.; Fortin, V.; Boilard, T.; Paradis, P.; Maes, F.; Talbot, L.; Vallée, R.; Bernier, M. 15 W monolithic fiber laser at 3.55 μm . *Opt. Lett.* **2021**, *47*, 289–292. [[CrossRef](#)]
12. Henderson-Sapir, O.; Jackson, S.D.; Ottaway, D.J. Versatile and widely tunable mid-infrared erbium doped ZBLAN fiber laser. *Opt. Lett.* **2016**, *41*, 1676–1679. [[CrossRef](#)] [[PubMed](#)]
13. Zhang, L.; Fu, S.; Sheng, Q.; Luo, X.; Zhang, J.; Shi, W.; Yao, J. Widely tunable single-frequency Er-doped ZBLAN fiber laser with emission from 3.37 to 3.72 μm . *Opt. Lett.* **2023**, *48*, 6200–6203. [[CrossRef](#)] [[PubMed](#)]
14. Lemieux-Tanguay, M.; Paradis, P.; Vallée, R.; Bernier, M. Watt-level Erbium-doped dual-wavelength pumped all-fiber laser at 3.8 μm . In Proceedings of the Optica Advanced Photonics Congress 2022, Barcelona, Spain, 11–15 December 2022.
15. Hudson, D.D.; Antipov, S.; Li, L.; Alamgir, I.; Hu, T.; Amraoui, M.E.; Messaddeq, Y.; Rochette, M.; Jackson, S.D.; Fuerbach, A. Toward all-fiber supercontinuum spanning the mid-infrared. *Optica* **2017**, *4*, 1163–1166. [[CrossRef](#)]
16. Tang, Y.; Wright, L.G.; Charan, K.; Wang, T.; Xu, C.; Wise, F.W. Generation of intense 100 fs solitons tunable from 2 to 4.3 μm in fluoride fiber. *Optica* **2016**, *3*, 948–951. [[CrossRef](#)]
17. Qin, Z.; Xie, G.; Ge, W.; Yuan, P.; Qian, L. Over 20-W mid-infrared picosecond optical parametric oscillator. *IEEE Photonics J.* **2015**, *7*, 1400506. [[CrossRef](#)]
18. Luo, H.; Yang, J.; Li, J.; Liu, Y. Widely tunable passively Q-switched Er³⁺-doped ZrF₄ fiber laser at the range of 3.4–3.7 μm based on Fe²⁺: ZnSe crystal. *Photon. Res.* **2019**, *7*, 1106–1111. [[CrossRef](#)]
19. Paradis, P.; Fortin, V.; Aydin, Y.O.; Vallée, R.; Bernier, M. 10 W-level gain-switched all-fiber laser at 2.8 μm . *Opt. Lett.* **2018**, *43*, 3196–3199. [[CrossRef](#)] [[PubMed](#)]
20. Luo, H.; Yang, J.; Liu, F.; Hu, Z.; Xu, Y.; Yan, F.; Peng, H.; Ouellette, F.; Li, J.; Liu, Y. Watt-level gain-switched fiber laser at 3.46 μm . *Opt. Express* **2019**, *27*, 1367–1375. [[CrossRef](#)] [[PubMed](#)]
21. Yang, J.; Luo, H.; Liu, F.; Li, J.; Liu, Y. Widely tunable gain-switched Er³⁺-doped ZrF₄ fiber laser from 3.4 to 3.7 μm . *IEEE Photon. Technol. Lett.* **2020**, *32*, 1335–1338. [[CrossRef](#)]

22. Zhang, L.; Fu, S.; Sheng, Q.; Luo, X.; Zhang, J.; Shi, W.; Yao, J. Pump quantum efficiency optimization of 3.5 μm Er-doped ZBLAN fiber laser for high-power operation. *Front. Optoelectron.* **2023**, *16*, 33. [[CrossRef](#)] [[PubMed](#)]
23. Zhang, L.; Zhang, J.; Sheng, Q.; Fu, S.; Li, Y.; Shi, C.; Shi, W.; Yao, J. Intracavity Tandemly-Pumped and Gain-Switched Tm-doped Fiber Laser at 1.7 μm . *J. Light. Technol.* **2022**, *40*, 4373–4378. [[CrossRef](#)]

Disclaimer/Publisher’s Note: The statements, opinions and data contained in all publications are solely those of the individual author(s) and contributor(s) and not of MDPI and/or the editor(s). MDPI and/or the editor(s) disclaim responsibility for any injury to people or property resulting from any ideas, methods, instructions or products referred to in the content.